THE JOURNAL OF PHYSICAL CHEMISTRY B

ARTICLE

pubs.acs.org/JPCB

Molecular Insight into Conformational Transition of Amyloid β-Peptide 42 Inhibited by (−)-Epigallocatechin-3-gallate Probed by Molecular Simulations

Fu-Feng Liu,[†] Xiao-Yan Dong,[†] Lizhong He,[‡] Anton P. J. Middelberg,[‡] and Yan Sun*[,†]

[†]Department of Biochemical Engineering and Key Laboratory of Systems Bioengineering of the Ministry of Education, School of Chemical Engineering and Technology, Tianjin University, Tianjin 300072, China

[‡]Centre for Biomolecular Engineering, Australian Institute for Bioengineering and Nanotechnology, The University of Queensland, QLD 4072, Australia

Supporting Information

ABSTRACT: Considerable experimental evidence indicates that (−)-epigallocatechin-3-gallate (EGCG) inhibits the fibrillogenesis of Aβ_{42} and alleviates its associated cytotoxicity. However, the molecular mechanism of the inhibition effect of EGCG on the conformational transition of Aβ_{42} remains unclear due to the limitations of current experimental techniques. In this work, molecular dynamics simulations and molecular mechanics-Poisson−Boltzmann surface area (MM-PBSA) analysis were coupled to better understand the issue. It was found that the direct interactions between EGCG and the peptide are the origin of its inhibition effects. Specifically, EGCG molecules expel water from the surface of the Aβ_{42}, cluster with each other, and interact directly with the peptide. The results of free energy decomposition calculated by MM-PBSA indicate that the nonpolar term contributes more than 71% to the binding free energy of the EGCG-Aβ_{42} complex, while polar interactions (i.e., hydrogen bonding) play a minor role. It was identified that there are 12 important residues of Aβ_{42} that strongly interact with EGCG (Phe4, Arg5, Phe19, Phe20, Glu22, Lys28, Gly29, Leu34-Gly37, and Ile41), while nonpolar interactions are mainly provided by the side chains of some hydrophobic residues (Phe, Met and Ile) and the main chains of some nonhydrophobic residues (Lys28 and Gly29). On the contrary, polar interactions are mainly formed by the main chain of Aβ_{42}, of which the main chains of Gly29 and Gly37 contribute greatly. The work has thus elucidated the molecular mechanism of the inhibition effect of EGCG on the conformational transition of Aβ_{42}, and the findings are considered critical for exploring more effective agents for the inhibition of Aβ_{42} fibrillogenesis.

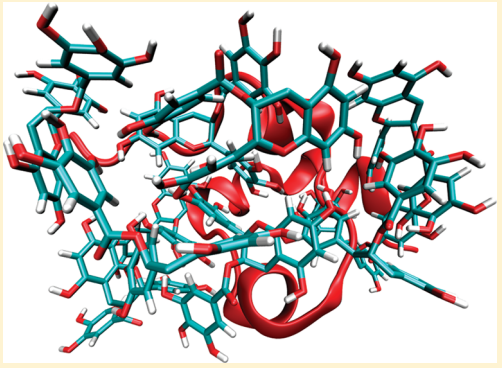

1. INTRODUCTION

Misfolding and aggregation of amyloid β-peptide (Aβ) is identified as a pathogenic process in Alzheimer's disease (AD).[1,2] Aβ is produced from an amyloid precursor protein through sequential cleavage by both β- and γ-secretase. There are several cutting sites on the amyloid precursor protein for γ-secretase, thus the length of Aβ is variable from 39 to 43 residues.[3] Among them, Aβ_{42} is the main culprit in the pathogenesis of AD because the peptides aggregate faster and the formed oligomers or protofibrils are significantly more neurotoxic than other Aβ segments.[4,5] So, the misfolding and aggregation of Aβ_{42} was hypothesized to impair synaptic function and initiate neuronal degeneration.[6,7] Previous experimental studies have found that the peptides first transform from their initial random coil or α-helix to β-sheet conformations and then form into various β-sheet-rich aggregated morphologies, suggesting that pathogenic β-sheet form drives the amyloid-assembly process.[8−10] This finding was also supported by molecular dynamics (MD) simulations, which demonstrated that increasing the stability of β-sheet conformation favors amyloid fibrillogenesis.[11−15] Therefore, preventing the conformational transition of Aβ monomer from initial random coil or α-helix into β-sheet is the primary goal of a number of therapeutic strategies under development or in clinical trials.

Recently, (−)-epigallocatechin-3-gallate (EGCG), the major polyphenolic component of green tea, has received special interest because of its inhibitory effect on amyloid fibril formation of Aβ,[16−20] α-synuclein,[21] prion protein Sup35,[22] and Huntington's protein.[23] For example, Ehrnhoefer et al.[24] have found that EGCG directly binds to the natively unfolded α-synuclein and Aβ_{42} and redirects the aggregation of these peptides to a disordered off-pathway reaction that results in the formation of unstructured, nontoxic amorphous aggregates. Despite some studies in thermodynamics,[25] kinetics and morphology,[18,24]

Received: March 21, 2011
Revised: September 6, 2011
Published: September 08, 2011

Table 1. The Detailed Information for the Different Simulated Systems

EGCG concentration (mol/L)	number of EGCG molecules	number of water molecules	simulation times (ns)
0	0	6930	300 × 3
0.04	5	6823	300 × 3
0.08	10	6714	300 × 4[a]

[a] One MD simulation is performed at 330 K, and the other three simulations are performed at 300 K.

a detailed atomic-level insight into the interactions between Aβ and EGCG is lacking.

Investigating the interactions between Aβ and EGCG presents a major opportunity, as it may lead to novel approaches in anti-AD drug discovery. However, it seems unlikely that experimental approaches can provide the molecular interactions between Aβ and EGCG, so here we use free energy decomposition based on MD simulation to address this issue. There are several successful methods to calculate the binding free energies of a given protein−ligand complex, such as free energy perturbation,[26,27] linear interaction energy,[28] and molecular mechanics Poisson−Boltzmann surface area (MM-PBSA).[29−33] MM-PBSA incorporates the effects of thermal averaging with a force field and continuum solvent models to postprocess a series of representative snapshots from MD trajectories. It can not only decompose different kinds of energies (e.g., electrostatic energy, van der Waals energy, solvation free energy, etc.) into residues, but also identify the driving forces and hot spots of a given protein−ligand complex.

Here, we investigated the molecular mechanism of the inhibition effect of EGCG on the conformational transition of Aβ_{42} addressed by a series of long time MD simulations and the MM-PBSA method. First, the conformational transition of the peptide at different EGCG concentrations was investigated. The preferential interactions between the peptide and EGCG were then studied, and the driving force was probed. Thereafter, the important residues of the peptide were discriminated according to the energy contribution of each residue using the MM-PBSA method. Finally, the origin of nonpolar interactions and hydrogen bonds (H-bonds) between Aβ_{42} and EGCG were probed. These observations are beneficial to understanding the inhibition mechanism of EGCG on the conformational transition of Aβ_{42} and designing new compounds for inhibiting the aggregation of Aβ.

2. METHODS

2.1. Parameterization of (−)-Epigallocatechin-3-gallate. The initial structure of EGCG was extracted from the Protein Data Bank (ID code 2KDH) (Figure S1a in the Supporting Information).[34] The GROMACS topology of EGCG was generated by the GlycoBioChem PRODRG2 Server (http://davapc1.bioch.dundee.ac.uk/prodrg/).[35] Lemkul et al.[36] have proven that atomic charges and charge groups of small molecules defined by PRODRG2 server were not correct, so atomic charges and charge groups of EGCG were all assigned based on the existing GROMOS96 53A6 force field parameter set.[37] Charges of aromatic hydroxyl groups were assigned based on tyrosine phenol group in the GROMOS96 53A6 force field. The charges of ether and ester groups, which do not exist in the force field, were taken from the GROMOS 53A6$_{OXY}$ force field parameter set developed by Horta et al.[38] A topology file for EGCG is provided in the Supporting Information. To validate the parameters assigned to EGCG, the value of octanol/water partition coefficient (log P) of EGCG was calculated using the thermodynamic integration (TI) method.[39] Detailed information about the log P calculation and the results of EGCG is also provided in the Supporting Information (See Sections S1 and S2).

2.2. Molecular Dynamics Simulation. Initial coordinates for the Aβ_{42} used in the simulations were taken from the NMR structures in hexafluoro-isopropanol (model 10, PDB entry 1IYT),[40] which has been used as the initial structure in many MD simulations for the structural characterization of Aβ in water.[41−43] The three-dimensional structure of Aβ_{42} shows two α-helix regions encompassing residues 8−25 and 28−38, connected through a flexible kink (Figure S1b in the Supporting Information).

An Aβ_{42} was first put in a cubic box with periodic boundary conditions. The size of the cubic box throughout the simulations was roughly 6 nm with negligible volume fluctuations. EGCG molecules were located and oriented randomly around the peptide. Then, water molecules nonoverlapping with either the peptide or EGCG molecules were randomly added into the simulation box. Finally, three positive ions (Na^+) were added by replacing the corresponding number of water molecules at the most negative electrical potential to achieve a neutral condition. After 1000 steps energy minimization, the system was first equilibrated for 100 ps under an isochoric−isothermal (NVT) ensemble using the Berendsen weak coupling method.[44] Then, it was further equilibrated for 100 ps under an isothermal−isobaric (NPT) ensemble using the Berendsen weak coupling method.[44] Position restraints were applied to the peptide during equilibration. Finally, production MD simulations were performed under NPT ensemble without any restraints. Temperature (300 or 330 K) and pressure (1 atm) were controlled by the Nosé−Hoover thermostat[45,46] and Parrinello−Rahman barostat,[47,48] respectively, which can generate a rigorous NPT ensemble.[49] To make certain that the effect of EGCG on the conformational transition of Aβ_{42} at different EGCG concentrations is the intrinsic character of EGCG rather than a stochastic output of simulations, three MD simulations of 300 ns were conducted for each system under different initial conditions by assigning different initial velocities on each atom of the simulation systems. Table 1 summarizes the important data for the different simulated systems.

All MD simulations were performed using the GROMACS 4.0.5 package[50] together with the GROMOS96 53A6 force field.[37] The simple point charge (SPC) model was used to describe water.[51] Newton's equations of motion were integrated using the leapfrog algorithm[52] with a 2 fs time step. The short-range van der Waals interactions were cut off at 1.4 nm. The long-range electrostatic interactions were treated with the particle mesh Ewald method,[53,54] with the real-space contribution to the Coulombic interactions truncated at 1.0 nm. The neighbor list was updated every five simulation steps. All bond lengths were constrained with the LINCS algorithm[55,56] with a relative geometric tolerance of 10^{-4}. Initial velocities were assigned according to a Maxwell distribution. For all simulations, the atomic coordinates were saved every 0.5 ps for analysis. MD simulations were run on a 160-CPU Dawning TC2600 blade server (Dawning, Tianjin, China).

2.3. Simulation Analyses. The simulation trajectories were analyzed using several auxiliary programs provided with the GROMACS 4.0.5 package. The programs include g_mindist

for calculating the number of contacts between the peptide and EGCG as a function of time, trjorder for the number of oxygen atoms of water and EGCG molecules around the surface of the peptide, and g_hbond for the number of H-bonds between the peptide and EGCG.

Simulation trajectories were visualized, and all of the snapshots in this article were prepared using the VMD software.[57] The simulation data plotted in the figures are averaged over three simulation trajectories, except those for secondary structures. Secondary structure analyses were carried out employing the dictionary secondary structure of protein (DSSP) method.[58] The secondary structures are calculated by only one trajectory, and the repeated trajectory showed similar results.

The time-averaged normalized ratio of water oxygen atoms, g_{NOW}, was used to interpret the local distribution of EGCG around the peptide.[59] g_{NOW} is computed by

$$g_{NOW} = \frac{n_{OW}(N_{OW} + N_{OE})}{(n_{OW} + n_{OE})N_{OW}} \quad (1)$$

where n_{OW} and n_{OE} are the local numbers of water oxygen atoms and hydroxyl group oxygen atoms of EGCG, respectively, located at a minimum distance from the closest atoms of Aβ_{42}; N_{OW} and N_{OE} denote the total numbers of water oxygen atoms and hydroxyl oxygen atoms of EGCG, respectively, in the simulation box.

2.4. Free Energy Decomposition. Per-residue free energy decomposition based on the MM-PBSA method was performed to address the contribution of each residue to the binding free energies of the Aβ_{42}−EGCG complex.[30] For Aβ_{42}−EGCG complex in 0.08 mol/L EGCG, 1000 snapshots were extracted from the last 100 ns trajectory of each simulation performed by GROMACS at the interval of 100 ps. These snapshots in GROMACS format were converted into CHARMM format using our in-house scripts, and were further analyzed by the MM-PBSA method using the CHARMM program.

Since the goal of MM-PBSA analysis is to identify the role of residues, the absolute binding free energy is not necessary, and the binding free energy (ΔG_{bind}) reported here is the relative binding free energy, which neglects the entropy contributions of the peptide. It was estimated as the sum of the gas phase energy (ΔG_{gas}) and the solvation energy (ΔG_{sol}), according to eq 2:

$$\Delta G_{bind} = \langle \Delta G_{gas} \rangle + \langle \Delta G_{sol} \rangle \quad (2)$$

The brackets, ⟨...⟩, indicate an average of an energy term along the MD simulation trajectory. G_{gas} contains an intermolecular electrostatic term (ΔG_{ele}), a van der Waals (vdW) term (ΔG_{vdw}), and an internal energy term (ΔG_{inter}). In this study, "the same trajectory method"[60] was used in all analyses. So, the internal energy term (ΔG_{inter}) is zero. Thus, ΔG_{gas} is the sum of ΔG_{ele} and ΔG_{vdw} (eq 3).

$$\Delta G_{gas} = \Delta G_{ele} + \Delta G_{vdw} \quad (3)$$

The solvation energy is divided into the polar solvation energy (G_{ps}) and the nonpolar solvation energy (G_{nps}) (eq 4).

$$G_{sol} = G_{ps} + G_{nps} \quad (4)$$

G_{ps} was calculated by solving the linear Poisson−Boltzmann (PB) equation using the PBEQ module of the CHARMM program. The solute and solvent dielectric constants were set to 1 and 80, respectively. The ionic strength was set to zero. G_{nps}, which could be considered as the sum of a solvent−solvent cavity term and a solute−solvent vdW term, was calculated according to eq 5:

$$G_{nps} = \gamma \times \mathrm{SASA} + b \quad (5)$$

The constants γ and b were set to 0.00542 kcal/(mol·Å^2) and 0.92 kcal/mol, respectively.[61] The solvent accessible surface area (SASA) was calculated using a water probe radius of 1.4 Å.

The binding free energy calculated by MM-PBSA is further decomposed into the contributions of residues. The free energy contribution of each residue ($G_{residue}$) contains polar (G_{polar}) and nonpolar interactions ($G_{nonpolar}$) according to eq 6, and each part is the sum of two energy terms, as given in eqs 7 and 8.

$$G_{residue} = G_{polar} + G_{nonpolar} \quad (6)$$

$$G_{polar} = G_{ele} + G_{ps} \quad (7)$$

$$G_{nonpolar} = G_{vdw} + G_{nps} \quad (8)$$

In the following analysis, G_{polar} is the sum of the intermolecular electrostatic energy (G_{ele}) and the electrostatic solvation energy (G_{ps}), as given in eq 7. And ΔG_{ele} is decomposed into residues according to eq 9. The linear PB equation allowed the decomposition of electrostatic solvation energy, since the electrostatic potential at point i (ϕ_i) can be calculated as the sum of the potentials created by other individual charges. The electrostatic contribution of residue j is estimated by summing over all charges q_i using the potential ϕ_i created at point i by the charges of residue j.

$$\Delta G^j_{elec} = \sum_{i \in \text{complex}} \frac{1}{2} q_i \phi_i^{j \in \text{complex}} - \left[\sum_{i \in Ig} \frac{1}{2} q_i \phi_i^{j \in Ig} + \sum_{i \in SpA} \frac{1}{2} q_i \phi_i^{j \in SpA} \right] \quad (9)$$

The vdW energy of each residue of Aβ_{42} was estimated as one-half of the vdW energy between itself and EGCG, and vice versa for EGCG. The division by two ensures that the sum of individual contributions represents the total vdW energy of the complex. The nonpolar solvation energy (G_{nps}) of each residue is taken to be proportional to the loss in SASA based on eq 5.

3. RESULTS AND DISCUSSION

3.1. Conformational Conversion of Aβ_{42} is Inhibited by EGCG. Previous experimental and theoretical studies have proven that conformational conversion from the initial α-helix to β-sheet is a crucial early step in Aβ amyloidogenesis.[62] To characterize the inhibition effect of EGCG on the conformational transition of Aβ_{42}, the secondary structure is determined by DSSP. The time evolution of the secondary structures of Aβ_{42} at different EGCG concentrations is shown in Figures 1 and S2−S4. Previous studies have shown that the GROMOS96 53A6 parameter set does not produce the correct balance of secondary structural elements, especially with respect to helices.[63−67] Therefore, all of the helices are summed and termed simply as α-helix. In water (Figures 1a and S2), the initial α-helix of Aβ_{42} decreased greatly from the initial value of 71.4% (Table 2) to about 47.0% after about 10 ns (Figure 1a). Especially, many residues of Helix II transform into a β-sheet/turn hybrid structure after several nanoseconds. For example, residues of $K_{28}G_{29}$, $I_{32}G_{33}$, and $V_{36}G_{37}$ mostly adopt short β-sheets linked with turn, which may be the intermediate state in the following aggregation process. In 0.04 mol/L

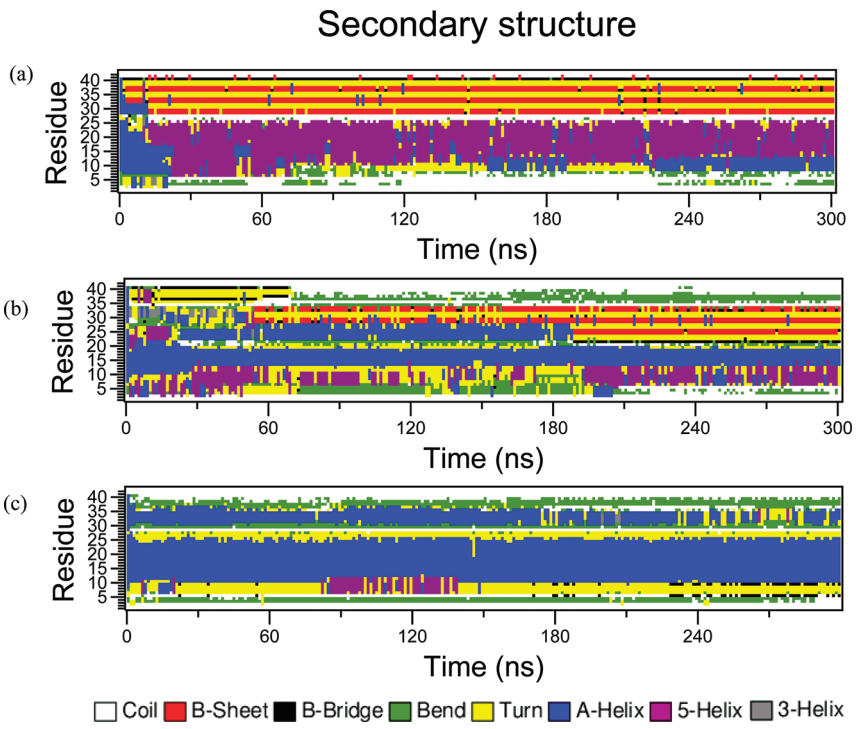

Figure 1. Evolution of the secondary structures of Aβ_{42} calculated by DSSP in water (a), 0.04 mol/L (b) and 0.08 mol/L (c) EGCG. The structure was analyzed every 0.6 ns. The vertical coordinate represents the residue number of Aβ_{42}, and the secondary structure is color-coded as indicated.

Table 2. Secondary Structure Compositions of Aβ_{42} in the Different Simulation Systems

secondary structure	initial value	water[a]	0.04 mol/L EGCG[a]	0.08 mol/L EGCG[a]
coil	9.5	21.8 ± 2.9	24.7 ± 3.1	20.6 ± 2.9
β-sheet	0	13.2 ± 3.6	12.2 ± 2.4	0
β-bridge	0	2.9 ± 1.9	2.8 ± 1.3	2.2 ± 2.4
α-helix[b]	71.4	39.4 ± 4.5	29.8 ± 5.6	45.3 ± 5.0
turn	4.8	18.3 ± 4.7	19.1 ± 5.0	17.0 ± 5.0
bend	14.3	4.5 ± 2.8	11.4 ± 3.3	14.9 ± 3.6

[a] Averaged data from the MD simulations of 200 to 300 ns. [b] The other helix (i.e., 5-helix and 3-helix) in Figures 1 and S2−S4 corresponds to the α-helix.

EGCG (EGCG/Aβ_{42} = 5) (Figures 1b and S3), the secondary structure of the peptide changed greatly, except the regions of H_{13}−F_{19}, which maintain their initial α-helix during the whole simulation. After 50 ns, $K_{28}G_{29}$ and $I_{32}G_{33}$ residues also form β-sheet structures linked with turn, but $V_{36}G_{37}$ residues transform into bend and coil. Moreover, the conformations of $V_{24}G_{25}$ also appear as a β-sheet structure after about 190 ns. At the end of the simulation, the percent content of β-sheet was about 12.2% (Table 2), suggesting that the conformational transition of Aβ_{42} was not inhibited in 0.04 mol/L EGCG.

When the peptide is simulated in 0.08 mol/L EGCG (EGCG/Aβ_{42} = 10) (Figures 1c and S4), the initial α-helix structure is well preserved in the entire 300 ns simulation, although it also decreases slightly as simulation time increases. It is remarkable that no β-sheet components are detected during the whole 300 ns simulation. In order to further validate if the inhibition effect of EGCG on the conformational transition of Aβ_{42} is correct, an MD simulation was performed at 330 K (Figure S4c in the Supporting Information). It is shown that the initial α-helix structure is well preserved, and the β-sheet does not exist in the entire 300 ns of simulation, which is consistent with the results of those at 300 K. Therefore, the conformational conversion from initial α-helix to β-sheet is completely inhibited in 0.08 mol/L EGCG.

The results depicted above implicate that EGCG inhibits conformational transition of Aβ_{42} in a dose-dependent manner. When the molar ratio of EGCG to Aβ_{42} is high enough, such as 10, the α-helical structure can be well preserved, and the formation of β-sheet structure is completely prevented.

3.2. EGCG Preferentially Interacts with Aβ_{42}. The initial configuration of the Aβ_{42}-EGCG system was obtained by uniformly distributing the EGCG molecules around the peptide within the simulation box. As EGCG molecules approach and interact with the peptide, the number of atomic contacts between EGCG and Aβ_{42} will increase. So, atomic contacts between EGCG and Aβ_{42} are used to represent the interactions between EGCG and the peptide, and are displayed as a function of simulation time in Figure 2a. It can be seen that the number of atomic contacts between the peptide and EGCG increases sharply within the first 20 ns (Figure 2a). Meanwhile, water molecules are released from the peptide surface, as indicated by a reduction of the number of water molecules in the first two solvation shells (Figure 2b). For example, the first solvation shell of the peptide

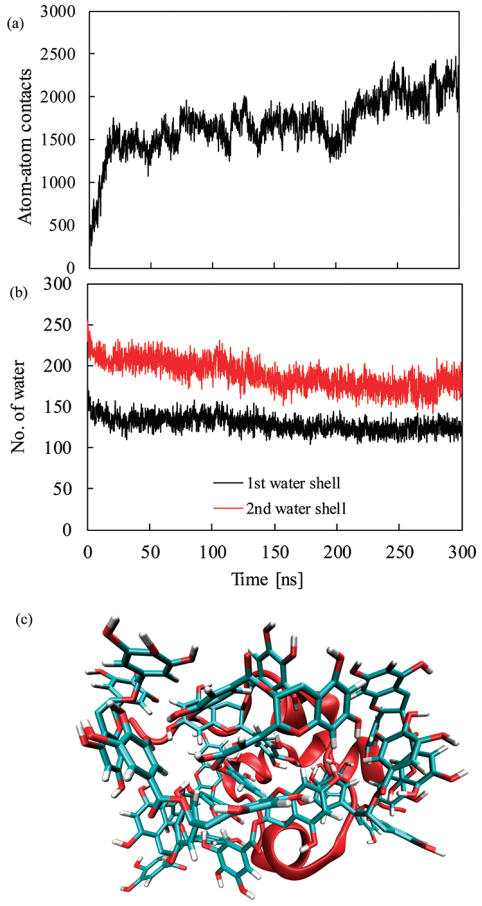

Figure 2. Time-development of properties of the peptide−EGCG system in 0.08 mol/L EGCG averaged over three simulations. (a) Atom contacts between the peptide and EGCG molecules (within 0.5 nm cutoff); (b) Number of water molecules in the first (0−0.34 nm) and second (0.34−0.5 nm) solvation shells of the peptide; (c) A representative structure of EGCG molecules bound to Aβ_{42} taken at 280 ns. For clarity, water molecules are not shown. The main chain of the peptide is shown by a red NewCartoon model, and EGCG is represented by a Licorice model. Atoms of EGCG are colored red for oxygen, white for hydrogen, and green for carbon. The snapshot is plotted with the visual molecular dynamics (VMD) software (http://www.ks.uiuc.edu/Research/vmd/).

loses about 40 water molecules, and the second solvation shell loses about 70 water molecules, within the first 20 ns. After binding to the peptide, EGCG molecules form stable atom-contacts with the peptide (∼2100, counting only contacts between EGCG and the peptide) (Figure 2a). In addition, the number of water molecules in the first two solvation shells becomes steady (Figure 2b). EGCG molecules eventually move toward the peptide surface, substitute the water molecules in the first two solvation shells, and interact with the peptide. This finding is consistent with the previous experimental observation that Aβ_{42} was targeted by EGCG and efficiently converted into stable aggregates.[18,24] Figure 2c shows a snapshot of EGCG binding with Aβ_{42} in 0.08 mol/L EGCG. It is clear that nine EGCG molecules cluster with each other, bind to the peptide, and form a stable aggregate.

The preferential interactions between Aβ_{42} and EGCG molecules can also be investigated by analyzing water and EGCG distributions. For this purpose, we characterized the relative local distribution of water and EGCG molecules from MD trajectories, according to the minimum distance of the water oxygen or of the

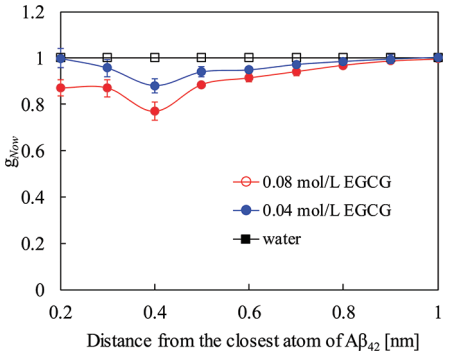

Figure 3. Time-averaged normalized ratio of water oxygen atoms, g_{NOW}, as a function of distance from the closest atom of Aβ_{42}.

polyphenol hydroxyl group oxygen from the closest peptide atoms. We computed the time-averaged normalized ratio of water oxygen atoms g_{NOW} (eq 1) in a similar way to Lerbret et al.[59] Class intervals are chosen at 0.1 nm thickness. From eq 1, we know that the ratio (g_{NOW}) is lower than 1 in the proximity of Aβ_{42} if EGCG preferentially interacts with the peptide. Conversely, the ratio is more than 1 if EGCG molecules are preferentially excluded from the surface of the peptide. Data are plotted only up to 1 nm from the closest atoms of the peptide; for distance larger than 1 nm, the distributions trail off due to irregular edge effects in the cubic box, which has no physical meaning.

Figure 3 shows g_{NOW} at different EGCG concentrations. It is obvious that EGCG molecules are enriched in the vicinity of the peptide with increasing EGCG concentration. For example, the g_{NOW} value is 0.997 in 0.04 mol/L EGCG, only a little less than unity, but it decreases to 0.870 in 0.08 mol/L EGCG. This finding means that some EGCG molecules exist around the surface of the peptide and directly interact with the peptide. In addition, the value of g_{NOW} shows a minimum (0.769 at EGCG = 0.08 mol/L) at about 0.4 nm, suggesting that EGCG molecules cluster with each other, form a continuous space-filling network, and surround the peptide at a distance of 0.4 nm. The direct interaction between EGCG molecules and the peptide is considered to be the origin of its inhibition effect on the conformational transition of Aβ_{42}.

3.3. Binding Free Energy Analysis of the Aβ_{42}−EGCG Complex. The results in section 3.2 have indicated that EGCG expels water from around Aβ_{42} and preferentially interacts with Aβ_{42}. To provide further insight into the interactions between EGCG and Aβ_{42}, the binding free energies for the Aβ_{42}−EGCG complex were evaluated using the MM-PBSA method. Due to its high computational demand, entropy contributions arising from changes in the degrees of freedom (translational, rotational, and vibrational) of the peptide are not included in the free energy calculation.[68] However, the contributions of the solvation are included in the polar and nonpolar solvation energy (eq 4).[60] In addition, the free energy decomposition is often used to identify the detailed interaction features and the hotspot residues of the binding surface.[60,69,70]

Table 3 lists nonpolar energy, $\Delta G_{nonpolar} = \Delta G_{vdw} + \Delta G_{nps}$, polar energy, $\Delta G_{polar} = \Delta G_{ele} + \Delta G_{ps}$, and the binding free energy, $\Delta G_{bind} = \Delta G_{nonpolar} + \Delta G_{polar}$. From Table 3, it is found that both nonpolar energy ($\Delta G_{nonpolar}$) and polar energy (ΔG_{polar}) are favorable for the formation of the EGCG−Aβ_{42} complex, but $\Delta G_{nonpolar}$ is over two times bigger than ΔG_{polar}, indicating that the nonpolar interactions play a major role (>71%). It is also

Table 3. Binding Free Energy Components of the Aβ_{42}−EGCG Complex

energetic components	Aβ_{42}−EGCG complex[a]
ΔG_{vdw}	−38.2
ΔG_{nps}	−6.0
ΔG_{ele}	−37.6
ΔG_{ps}	19.9
$\Delta G_{nonpolar}$[b]	−44.2
ΔG_{polar}[c]	−17.7
ΔG_{bind}[d]	−61.9

[a] Unit: kcal/mol. [b] $\Delta G_{nonpolar} = \Delta G_{vdw} + \Delta G_{nps}$, nonpolar energy. [c] $\Delta G_{polar} = \Delta G_{ele} + \Delta G_{ps}$, polar energy. [d] $\Delta G_{bind} = \Delta G_{nonpolar} + \Delta G_{polar}$, in which the entropy contributions of the peptide is not included.

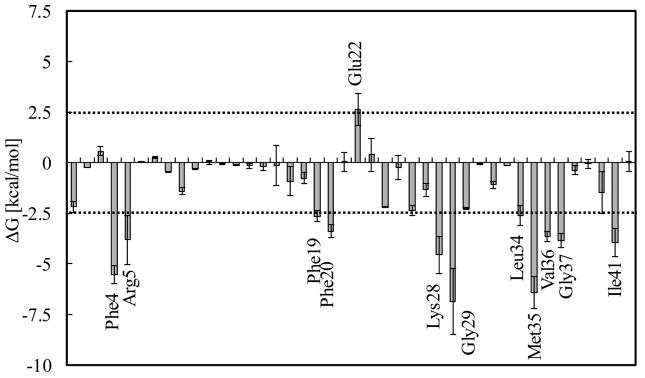

Figure 4. Binding free energy contribution of each residue of Aβ_{42} in the EGCG−Aβ_{42} complex. The residues with the most favorable (< −2.5 kcal/mol) or unfavorable (>2.5 kcal/mol) contributions are labeled.

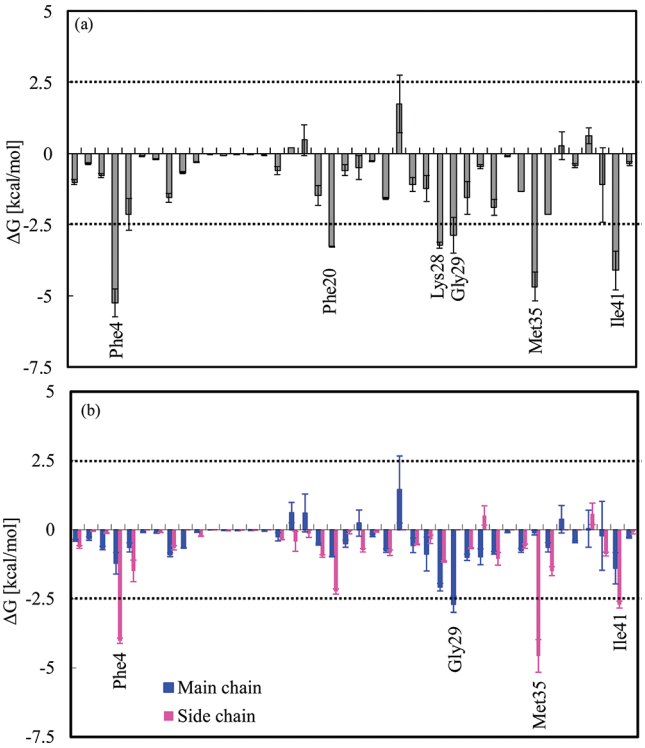

Figure 5. The nonpolar contribution of each residue of Aβ_{42} (a), and the nonpolar energies decomposed into the contributions of main chain and side chain (b). The residues with the most favorable (< −2.5 kcal/mol) or unfavorable (> 2.5 kcal/mol) contributions are labeled.

found that both the van der Waals energy (ΔG_{vdw}) and nonpolar solvation term (ΔG_{nps}) are favorable for EGCG binding, but the ΔG_{vdw} term (−38.2 kcal/mol) takes more than 86% of the contribution to $\Delta G_{nonpolar}$. In contrast to the nonpolar part in ΔG_{bind}, the two components of the polar free energy (ΔG_{ele} and ΔG_{ps}) behave oppositely. Namely, the ΔG_{ele} contribution (−37.6 kcal/mol) is favorable for the binding process, while the ΔG_{ps} term (19.9 kcal/mol) works for unbinding. So, the counterplay between the two components of ΔG_{polar} greatly weakens the contribution of polar interactions.

As we know, EGCG (Figure S1a in the Supporting Information) contains three aromatic rings that can induce hydrophobic association with other hydrophobic groups, and Aβ_{42} contains many hydrophobic residues (such as, Phe, Leu, Met, Val, and Ile). Meanwhile, the phenyl ring in residue Phe and EGCG can lead to strong nonpolar interactions through $\pi-\pi$ stacking interactions. It can thus be concluded that nonpolar interactions play a major role in the binding of EGCG to Aβ42, although both nonpolar and polar interactions are favorable for the formation of the EGCG−Aβ42 complex.

3.4. Free Energy Decomposition for Aβ_{42}. In order to find the important residues of Aβ_{42} interacting with EGCG, the free energy decomposition for each residue was carried out, and the results are represented in Figure 4. In the free energy decomposition analysis, the important residues are defined as those whose absolute value of free energy contribution is larger than 2.5 kcal/mol. The criterion of 2.5 kcal/mol is mostly employed in the literature.[60,71] It can be seen from Figure 4 that most of the residues provide favorable binding free energies. Among them, 12 residues, Phe4, Arg5, Phe19, Phe20, Glu22, Lys28, Gly29, Leu34-Gly37, and Ile41, contribute greatly, and, except for Glu22, 11 of them provide favorable binding free energies.

From section 3.3, it is clear that there are two components to the energy of interaction (nonpolar and polar energies) between EGCG and Aβ_{42}. In order to identify the detailed contribution of each residue, the energy contribution was decomposed into nonpolar and polar energies. Moreover, to reveal the origin of the nonpolar and polar energies, the energy contribution of each residue was further decomposed into two parts separately offered by the main chain and side chain. First, we analyzed the nonpolar energies between EGCG and Aβ_{42}. Figure 5 shows the nonpolar contributions of per-residue and decomposition into those from the main chain and side chains. Figure 5a shows that most of the residues provide favorable nonpolar interactions. Especially, six residues (Phe4, Phe20, Lys28, Gly29, Met35, and Ile41) are verified to have effective nonpolar interaction contribution (ΔG < −2.5 kcal/mol). From Figure 5b, it is found that the nonpolar energies mainly originate from the side chains of the residues, accounting for almost 60% of the nonpolar energies. For example, nonpolar interactions of Phe4, Met35, and Ile41 mainly come from their hydrophobic side chains. On the contrary, the nonpolar interactions of Gly29 are contributed by its main chain. It is caused by the tight contact with EGCG because Gly29 does not possess a side chain. As for Lys28, the nonpolar interactions are provided by both the main chain and the side chain, of which the main chain contributes more (>64%). As defined in eq 8, nonpolar energy is composed of van der Waals energy (ΔG_{vdw}) and nonpolar solvation term (ΔG_{nps}). The van der Waals forces

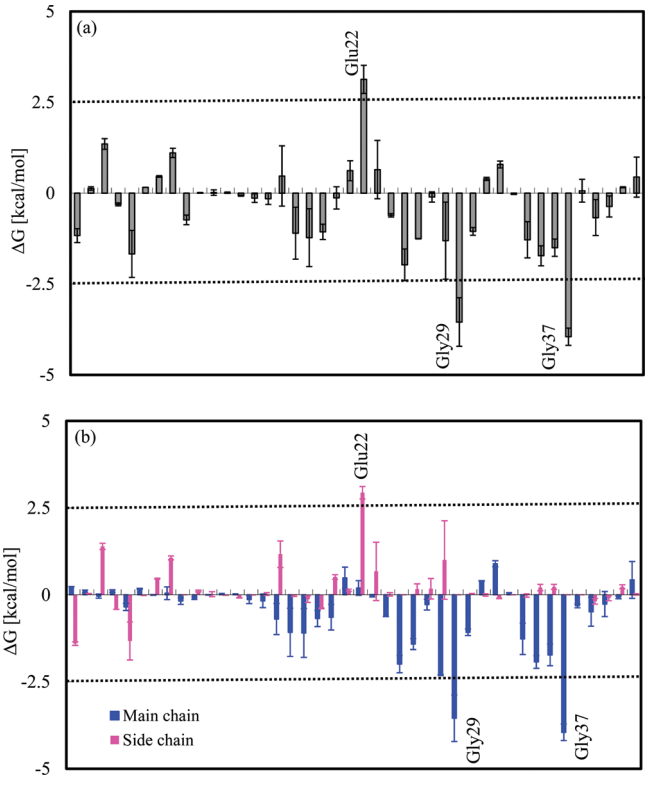

Figure 6. The polar contribution of each residue of Aβ_{42} (a) and the polar energies decomposed into the contributions of main chain and side chain (b). The residues with the most favorable (< −2.5 kcal/mol) or unfavorable (> 2.5 kcal/mol) contributions are labeled.

cause relatively weak attraction between neutral atoms and molecules arising from polarization induced in each particle by the presence of other particles. Generally, there is a van der Waals interaction when the distance between two atoms is 0.4 to 0.6 nm. In the case of Lys28, ΔG_{nps} of the main chain is relatively weak because the main chain of the peptide is polar. Therefore, the nonpolar energy of the main chain is dominated by the van der Waals term. As shown in Table 3, the ΔG_{vdw} term actually comprises more than 86% contribution to $\Delta G_{nonpolar}$. In other words, the main chain of the Lys28 contributes to strong nonpolar energy through the van der Waals forces, although the main chain of the peptide is polar. Hence, the nonpolar interactions between EGCG and Aβ_{42} are mainly provided by the side chains of some hydrophobic residues (e.g., Phe4, Phe20, Met35, and Ile41) and the main chains of some nonhydrophobic residues (e.g., Lys28 and Gly29).

Figure 6 shows the free energy decomposition results of polar energies for Aβ_{42}. It can be seen that only three residues (Glu22, Gly29, and Gly37) make distinct contributions, while the other residues have a relatively small effect (Figure 6a). Of the three residues, Gly29 and Gly37 offer favorable polar energies, while Glu22 contributes reversely to the peptide−EGCG binding. The polar energies were further divided into the contributions of main chain and side chain of each residue (Figure 6b). From the figure, we can conclude that the main chain of the peptide provides the majority of the favorable polar energy (−23.3 kcal/mol), which is caused by its polarity, and it can form hydrogen bonds with EGCG. For example, atoms O, N, and H of the peptide bond can form H-bonds with the hydroxyl groups of EGCG.

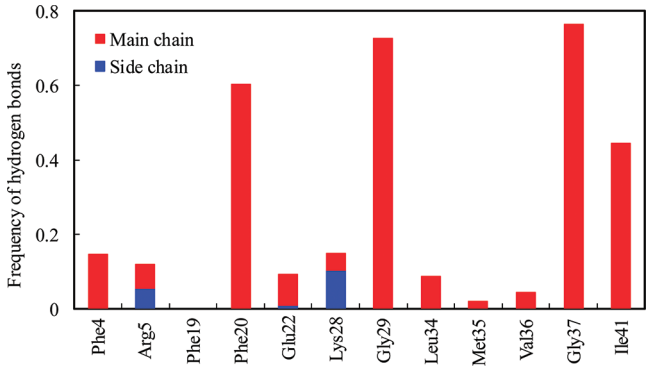

Figure 7. Occupancy of hydrogen bonds between the important residues of Aβ_{42} and EGCG.

On the contrary, the side chains of the residues offer unfavorable polar energies (6.39 kcal/mol). Particularly, the unfavorable polar energy between the side chain of Glu22 and EGCG is as high as 3.13 kcal/mol. It is mainly caused by its negatively charged side chain (2.94 kcal/mol), which can lead to large positive solvation energy.

From the above analysis, it is concluded that nonpolar interactions are largely provided by the side chains of some hydrophobic residues (e.g., Phe4, Phe20, Met35 and Ile41) and the main chains of Lys28 and Gly29, while polar interactions are mainly given by the main chain of the peptide, with the main chains of Gly29 and Gly37 contributing greatly.

3.5. Effects of Hydrogen Bonds and Nonpolar Interactions. In section 3.4, we have proven that there exist polar interactions between EGCG and Aβ_{42}. As we know, EGCG has zero net charge and is an aromatic compound with eight hydroxyl groups (Figure S1a in the Supporting Information). This suggests that it may interact with the peptide by H-bonds involving its hydroxyl groups.[25,72] To examine the H-bonds between EGCG and Aβ_{42}, the occupancies of all possible H-bonds between the important residues of the peptide and EGCG were measured by calculating the percentage of time during the simulation that the H-bonds existed. Herein, H-bonds are defined as the donor-to-acceptor distance less than 0.35 nm and the donor−hydrogen−acceptor angle within 30° of linearity.

Figure 7 shows the occupancies of H-bonds between EGCG and the 12 important residues of Aβ_{42} as identified in Figure 4. It can be seen that three residues (Phe20, Gly29, and Gly37) interact with EGCG via H-bonds with high occupancies (> 60%). Additionally, it is found that the majority of H-bonds exist between EGCG and the main chain of Aβ_{42}. Residues Gly29 and Gly37 spend more than 60% of its time in the formation of H-bonds with EGCG. It is due to the absence of a side chain in glycine, making EGCG interact easily with the main chains of these residues. For the hydrophobic residues (Phe, Leu, Met, Val, and Ile), EGCG also interacts with their main chains by H-bonds. Previous investigations have demonstrated that the aggregation and oligomerization of Aβ peptides are dominated by hydrophobic interactions and H-bonds.[73] In this study, we have used MD and MM-PBSA to systematically analyze the interactions between EGCG and Aβ_{42}. Our data indicate that nonpolar interactions and H-bonds are coupled to prevent the conformational conversion of Aβ_{42} and its following aggregation.

It is considered that there are two kinds of effects of nonpolar interactions and H-bonds. One is that the two kinds of interactions

are provided by the same residue. Especially for hydrophobic residues, they provide not only strong nonpolar interactions via their side chains but also powerful H-bonds via their main chains. For example, hydrophobic residues Phe20 and Ile41 provide both of nonpolar interactions and H-bonds with EGCG via their side chains and main chains, respectively. The other one is that the two kinds of interactions are provided by the multiresidues. That is, some hydrophobic residues (Phe, Leu, Val, and Met) can provide nonpolar interactions via their side chains. At the same time, the main chains of the neighboring polar residues interact with EGCG via H-bonds. For example, EGCG interacts with the side chains of Met35 and Val36 via nonpolar interactions (Figure 5b). Meanwhile, the main chain of Gly37 interacts with EGCG via H-bonds (Figures 6b and 7). So, EGCGs have strong interactions and tightly bind with these residues (Met35, Val36 and Gly37). The nonpolar interactions and H-bonds lead to the tight binding and the inhibition of the conformational conversion of Aβ_{42}.

Our MD studies indicate that EGCG is very effective at inhibiting the conformational transition of Aβ_{42}, thus preventing the formation of β-sheet structure. In addition, in vitro studies have proven that EGCG can redirect the aggregation cascade of Aβ_{42} and inhibit the formation of toxic, β-sheet-rich oligomers or protofibrils.[24] It has been demonstrated that radioactively labeled EGCG can be detected in mouse brains after oral administration.[74] These results suggest that EGCG may have considerable potential as drug candidates for the therapy of AD.

As we know, EGCG is notoriously insoluble in water. It may be impossible for 0.08 mol/L EGCG to reach a patient's brain. The reason to use such a high concentration in this work is to facilitate MD simulations. The concentration of Aβ42 is 15 μmol/L in experimental studies,[23] only 1/466 of that in our simulations (7 mmol/L). A system with such a low peptide concentration cannot be simulated with current computation capability because it will need a very large box containing one single peptide and very huge amount of water molecules. In order to reduce the computational cost associated with MD simulation of protein, the strategy of using a higher solute concentration and elevated temperature has often been utilized. The strategy has successfully been used to investigate the interactions between ligand and the target protein.[75,76] For example, Wu et al.[77] identified and characterized two specific binding modes of Congo red molecules to protofibrils formed by the peptide (GNNQQNY) using all-atom MD simulations. The concentration of the protofibrils and Congo red (~7 mmol/L) in their MD simulation was about 1000-fold higher than the typical experimental concentrations (~8 μmol/L), and the simulation results were in good agreement with those of corresponding experiments. Herein, we also used the similar strategy. EGCG (0.08 mol/L) was about 500-fold higher than the typical experiment concentrations (150 μmol/L). Importantly, the concentration ratio of inhibitor to peptide is kept the same as the experimental result.[24] Therefore, we expect that the inhibition mechanism observed in the present system is relevant in vivo.

4. CONCLUSIONS

MD simulations, MM-PBSA free energy calculations, and decompositions for the Aβ_{42}−EGCG complex have been performed for identifying the molecular interactions between EGCG and Aβ_{42} and exploring the molecular mechanism of the inhibition effect of EGCG on the conformational transition of the peptide. It is confirmed that the conformational transition of Aβ_{42} is inhibited by EGCG in a dose-dependent manner. In water and low-concentration EGCG solutions, the conformational transition of Aβ_{42} from its initial α-helix to β-sheet is observed. By increasing EGCG concentration to EGCG/Aβ_{42} = 10, the structures with β-sheet components are completely prevented. The function of EGCG results from its direct binding to the peptide. Namely, EGCG replaces water from the surface of Aβ_{42} and interacts directly with the peptide. The results of free energy calculation indicate that nonpolar and polar interactions are both favorable for the binding of EGCG. Of them, the dominant contribution to the interactions comes from the nonpolar interactions (>70%) offered mainly by the van der Waals term. By free energy decomposition, it is found that the residues Phe4, Arg5, Phe19, Phe20, Glu22, Lys28, Gly29, Leu34-Gly37, and Ile41 contribute significantly to the interactions between EGCG and Aβ42. In addition, the nonpolar interactions mainly come from the side chains of some hydrophobic residues and the main chains of some nonhydrophobic residues. On the contrary, the polar interactions (H-bonds) are provided by the main chain of Aβ_{42}. Finally, we have summarized that the conformational transition of the peptide is inhibited by both the nonpolar interactions and H-bonds between EGCG and Aβ_{42}. This work has thus elucidated the molecular mechanism of the interactions between EGCG and Aβ_{42}, and will lead to new opportunities toward the development of more effective agents for the inhibition of Aβ oligomeric aggregation.

■ ASSOCIATED CONTENT

Supporting Information. The chemical structure of EGCG and the initial structure of Aβ_{42}, the methods for the calculation of EGCG's log *P*, and the results and discussion for the parametrization of EGCG are provided. The GROMACS topology data for EGCG are given in a separate text. This material is available free of charge via the Internet at http://pubs.acs.org.

■ AUTHOR INFORMATION

Corresponding Author

*Phone: +86 22 27404981. Fax: +86 22 27406590. E-mail: ysun@tju.edu.cn.

■ ACKNOWLEDGMENT

This work was supported by the Natural Science Foundation of China (Nos. 20876111 and 20906068), the National Basic Research Program of China (973 Program, No. 2009CB724705) and the Natural Science Foundation of Tianjin from Tianjin Municipal Science and Technology Commission (Contract No. 10JCYBJC04500). The authors thank Dr. Justin A. Lemkul for advice regarding log *P* calculations.

■ REFERENCES

(1) Mason, J. M.; Kokkoni, N.; Stott, K.; Doig, A. J. *Curr. Opin. Struct. Biol.* **2003**, *13*, 526–532.
(2) Jakob-Roetne, R.; Jacobsen, H. *Angew. Chem., Int. Ed.* **2009**, *48*, 3030–3059.
(3) Selkoe, D. J. *Nat. Cell Biol.* **2004**, *6*, 1054–1061.
(4) Haass, C.; Selkoe, D. J. *Nat. Rev. Mol. Cell Biol.* **2007**, *8*, 101–112.

(5) Ahmed, M.; Davis, J.; Aucoin, D.; Sato, T.; Ahuja, S.; Aimoto, S.; Elliott, J. I.; Van Nostrand, W. E.; Smith, S. O. *Nat. Struct. Mol. Biol.* **2010**, *17*, 561–567.
(6) Hardy, J.; Selkoe, D. J. *Science* **2002**, *297*, 353–356.
(7) Sakono, M.; Zako, T. *FEBS J.* **2010**, *277*, 1348–1358.
(8) Zhuang, W.; Sgourakis, N. G.; Li, Z.; Garcia, A. E.; Mukamel, S. *Proc. Natl. Acad. Sci. U.S.A.* **2010**, *107*, 15687–15692.
(9) Jang, S.; Shin, S. *J. Phys. Chem. B* **2006**, *110*, 1955–1958.
(10) Yang, D. S.; Yip, C. M.; Huang, T. H.; Chakrabartty, A.; Fraser, P. E. *J. Biol. Chem.* **1999**, *274*, 32970–32974.
(11) Wei, G.; Jewett, A. I.; Shea, J. E. *Phys. Chem. Chem. Phys.* **2010**, *12*, 3622–3629.
(12) Pellarin, R.; Caflisch, A. *J. Mol. Biol.* **2006**, *360*, 882–892.
(13) Bellesia, G.; Shea, J. E. *J. Chem. Phys.* **2009**, *130*, 145103–145110.
(14) Xu, Y.; Shen, J.; Luo, X.; Zhu, W.; Chen, K.; Ma, J.; Jiang, H. *Proc. Natl. Acad. Sci. U.S.A.* **2005**, *102*, 5403–5407.
(15) Urbanc, B.; Cruz, L.; Yun, S.; Buldyrev, S. V.; Bitan, G.; Teplow, D. B.; Stanley, H. E. *Proc. Natl. Acad. Sci. U.S.A.* **2004**, *101*, 17345–17350.
(16) Lin, C. L.; Chen, T. F.; Chiu, M. J.; Way, T. D.; Lin, J. K. *Neurobiol. Aging* **2009**, *30*, 81–92.
(17) Rezai-Zadeh, K.; Arendash, G. W.; Hou, H.; Fernandez, F.; Jensen, M.; Runfeldt, M.; Shytle, R. D.; Tan, J. *Brain Res.* **2008**, *1214*, 177–187.
(18) Bieschke, J.; Russ, J.; Friedrich, R. P.; Ehrnhoefer, D. E.; Wobst, H.; Neugebauer, K.; Wanker, E. E. *Proc. Natl. Acad. Sci. U.S.A.* **2010**, *107*, 7710–7715.
(19) Guo, J. P.; Yu, S.; McGeer, P. L. *J. Alzheimer's Dis.* **2010**, *19*, 1359–1370.
(20) Choi, Y. T.; Jung, C. H.; Lee, S. R.; Bae, J. H.; Baek, W. K.; Suh, M. H.; Park, J.; Park, C. W.; Suh, S. I. *Life Sci.* **2001**, *70*, 603–614.
(21) Waxman, E. A.; Emmer, K. L.; Giasson, B. I. *Biochem. Biophys. Res. Commun.* **2010**, *391*, 1415–1420.
(22) Roberts, B. E.; Duennwald, M. L.; Wang, H.; Chung, C.; Lopreiato, N. P.; Sweeny, E. A.; Knight, M. N.; Shorter, J. *Nat. Chem. Biol.* **2009**, *5*, 936–946.
(23) Ehrnhoefer, D. E.; Duennwald, M.; Markovic, P.; Wacker, J. L.; Engemann, S.; Roark, M.; Legleiter, J.; Marsh, J. L.; Thompson, L. M.; Lindquist, S.; Muchowski, P. J.; Wanker, E. E. *Hum. Mol. Genet.* **2006**, *15*, 2743–2751.
(24) Ehrnhoefer, D. E.; Bieschke, J.; Boeddrich, A.; Herbst, M.; Masino, L.; Lurz, R.; Engemann, S.; Pastore, A.; Wanker, E. E. *Nat. Struct. Mol. Biol.* **2008**, *15*, 558–566.
(25) Wang, S. H.; Liu, F. F.; Dong, X. Y.; Sun, Y. *J. Phys. Chem. B* **2010**, *114*, 11576–11583.
(26) Zwanzig, R. W. *J. Chem. Phys.* **1954**, *22*, 1420–1426.
(27) Reddy, M. R.; Erion, M. D. *J. Am. Chem. Soc.* **2001**, *123*, 6246–6252.
(28) Aqvist, J.; Medina, C.; Samuelsson, J. E. *Protein Eng.* **1994**, *7*, 385–391.
(29) Srinivasan, J.; Cheatham, T. E., III; Cieplak, P.; Kollman, P. A.; Case, D. A. *J. Am. Chem. Soc.* **1998**, *120*, 9401–9409.
(30) Kollman, P. A.; Massova, I.; Reyes, C.; Kuhn, B.; Huo, S.; Chong, L.; Lee, M.; Lee, T.; Duan, Y.; Wang, W.; Donini, O.; Cieplak, P.; Srinivasan, J.; Case, D. A.; Cheatham, T. E., III. *Acc. Chem. Res.* **2000**, *33*, 889–897.
(31) Deng, N. J.; Cieplak, P. *Phys. Chem. Chem. Phys.* **2009**, *11*, 4968–4981.
(32) Treesuwan, W.; Wittayanarakul, K.; Anthony, N. G.; Huchet, G.; Alniss, H.; Hannongbua, S.; Khalaf, A. I.; Suckling, C. J.; Parkinson, J. A.; Mackay, S. P. *Phys. Chem. Chem. Phys.* **2009**, *11*, 10682–10693.
(33) Hou, T.; Wang, J.; Li, Y.; Wang, W. *J. Chem. Inf. Model.* **2011**, *51*, 69–82.
(34) Robertson, I. M.; Li, M. X.; Sykes, B. D. *J. Biol. Chem.* **2009**, *284*, 23012–23023.
(35) Schuttelkopf, A. W.; van Aalten, D. M. *Acta Crystallogr. D* **2004**, *60*, 1355–1363.
(36) Lemkul, J. A.; Allen, W. J.; Bevan, D. R. *J. Chem. Inf. Model.* **2010**, *50*, 2221–2235.
(37) Oostenbrink, C.; Villa, A.; Mark, A. E.; van Gunsteren, W. F. *J. Comput. Chem.* **2004**, *25*, 1656–1676.
(38) Horta, B. A. C.; Fuchs, P. F. J.; van Gunsteren, W. F.; Hunenberger, P. H. *J. Chem. Theory. Comput.* **2011**, *7*, 1016–1031.
(39) Lemkul, J. A.; Bevan, D. R. *Biochemistry* **2010**, *49*, 3935–3946.
(40) Crescenzi, O.; Tomaselli, S.; Guerrini, R.; Salvadori, S.; D'Ursi, A. M.; Temussi, P. A.; Picone, D. *Eur. J. Biochem.* **2002**, *269*, 5642–5648.
(41) Triguero, L.; Singh, R.; Prabhakar, R. *J. Phys. Chem. B* **2008**, *112*, 7123–7131.
(42) Lee, C.; Ham, S. *J. Comput. Chem.* **2011**, *32*, 349–355.
(43) Bora, R. P.; Prabhakara, R. *J. Chem. Phys.* **2009**, *131*, 155103.
(44) Berendsen, H. J. C.; Postma, J. P. M.; van Gunsteren, W. F.; DiNola, A.; Haak, J. R. *J. Chem. Phys.* **1984**, *81*, 3684–3690.
(45) Nosé, S. *J. Chem. Phys.* **1984**, *81*, 511–519.
(46) Hoover, W. G. *Phys. Rev. A* **1985**, *31*, 1695–1697.
(47) Parrinello, M.; Rahman, A. *J. Appl. Phys.* **1981**, *52*, 7182–7190.
(48) Nosé, S.; Klein, M. L. *Mol. Phys.* **1983**, *50*, 1055–1076.
(49) Lemkul, J. A.; Bevan, D. R. *J. Phys. Chem. B* **2010**, *114*, 1652–1660.
(50) Van Der Spoel, D.; Lindahl, E.; Hess, B.; Groenhof, G.; Mark, A. E.; Berendsen, H. J. *J. Comput. Chem.* **2005**, *26*, 1701–1718.
(51) Berendsen, H. J. C.; Postma, J. P. M.; van Gunsteren, W. F.; Hermans, J., In *Intermolecular Forces*; Pullman, B., Ed.; Reidel: Dordecht, Holland, 1981; p 331.
(52) Verlet, L. *Phys. Rev.* **1967**, *159*, 98–103.
(53) Darden, T.; York, D.; Pedersen, L. *J. Chem. Phys.* **1993**, *98*, 10089–10092.
(54) Essman, U.; Perera, L.; Berkowitz, M. L.; Darden, T.; Lee, H.; Pedersen, L. G. *J. Chem. Phys.* **1995**, *103*, 8577–8593.
(55) Hess, B.; Berendsen, H. J. C.; Fraaije, J. G. E. M. *J. Comput. Chem.* **1997**, *18*, 1463–1472.
(56) Hess, B. *J. Chem. Theory. Comput.* **2008**, *4*, 116–122.
(57) Humphrey, W.; Dalke, A.; Schulten, K. *J. Mol. Graph.* **1996**, *14* (33−38), 27–38.
(58) Kabsch, W.; Sander, C. *Biopolymers* **1983**, *22*, 2577–2637.
(59) Lerbret, A.; Bordat, P.; Affouard, F.; Hedoux, A.; Guinet, Y.; Descamps, M. *J. Phys. Chem. B* **2007**, *111*, 9410–9420.
(60) Zoete, V.; Meuwly, M.; Karplus, M. *Proteins* **2005**, *61*, 79–93.
(61) Gorfe, A. A.; Jelesarov, I. *Biochemistry* **2003**, *42*, 11568–11576.
(62) Cerda-Costa, N.; Esteras-Chopo, A.; Aviles, F. X.; Serrano, L.; Villegas, V. *J. Mol. Biol.* **2007**, *366*, 1351–1363.
(63) Nguyen, P. H.; Li, M. S.; Derreumaux, P. *Phys. Chem. Chem. Phys.* **2011**, *13*, 9778–9788.
(64) Project, E.; Nachliel, E.; Gutman, M. *J. Comput. Chem.* **2010**, *31*, 1864–1872.
(65) Cao, Z.; Lin, Z.; Wang, J.; Liu, H. *J. Comput. Chem.* **2009**, *30*, 645–660.
(66) Matthes, D.; de Groot, B. L. *Biophys. J.* **2009**, *97*, 599–608.
(67) Marklund, E. G.; Larsson, D. S.; van der Spoel, D.; Patriksson, A.; Caleman, C. *Phys. Chem. Chem. Phys.* **2009**, *11*, 8069–8078.
(68) Numata, J.; Wan, M.; Knapp, E. W. *Genome Inf.* **2007**, *18*, 192–205.
(69) Huang, B.; Liu, F. F.; Dong, X. Y.; Sun, Y. *J. Phys. Chem. B* **2011**, *115*, 4168–4176.
(70) Zeng, J.; Li, W.; Zhao, Y.; Liu, G.; Tang, Y.; Jiang, H. *J. Phys. Chem. B* **2008**, *112*, 2719–2726.
(71) Lafont, V.; Schaefer, M.; Stote, R. H.; Altschuh, D.; Dejaegere, A. *Proteins* **2007**, *67*, 418–434.
(72) Maiti, T. K.; Ghosh, K. S.; Dasgupta, S. *Proteins* **2006**, *64*, 355–362.
(73) Favrin, G.; Irback, A.; Mohanty, S. *Biophys. J.* **2004**, *87*, 3657–3664.
(74) Suganuma, M.; Okabe, S.; Oniyama, M.; Tada, Y.; Ito, H.; Fujiki, H. *Carcinogenesis* **1998**, *19*, 1771–1776.
(75) Wu, C.; Lei, H.; Wang, Z.; Zhang, W.; Duan, Y. *Biophys. J.* **2006**, *91*, 3664–3672.
(76) Liu, F. F.; Ji, L.; Dong, X. Y.; Sun, Y. *J. Phys. Chem. B* **2009**, *113*, 11320–11329.
(77) Wu, C.; Wang, Z.; Lei, H.; Zhang, W.; Duan, Y. *J. Am. Chem. Soc.* **2007**, *129*, 1225–1232.